Evaluation of regional estimates of winter wheat yield by assimilating three remotely sensed reflectance datasets into the coupled WOFOST–PROSAIL model

Jianxi HUANG[a,b †], Hongyuan MA[a], Fernando SEDANO[c], Phillip LEWIS[d], Shunlin LIANG[c,e], Qingling WU[d], Wei SU[a,b], Xiaodong ZHANG[a,b], Dehai ZHU[a,b]

[a] College of Land Science and Technology, China Agricultural University, Beijing, 100083, China.

[b] Key Laboratory of Remote Sensing for Agri-Hazards, Ministry of Agriculture, Beijing 100083, China

[c] Department of Geographical Sciences, University of Maryland, College Park MD 20742, USA

[d] Department of Geography, University College London, and National Centre for Earth Observation, Gower St., London, WC1E 6BT, UK

[e] State Key Laboratory of Remote Sensing Science, School of Geography, Beijing Normal University, Beijing, 100875, China

[†] Corresponding author – Jianxi Huang, College of Land Science and Technology, China Agricultural University, No. 17 Qinghua East Road, Haidian District, Beijing, 100083, China. E-mail: jxhuang@cau.edu.cn; Tel.: +86 010-6273-7855, Fax: +86 010-6273-7855

Abstract

To estimate regional-scale winter wheat (*Triticum aestivum*) yield, we developed a data-assimilation scheme that assimilates remote-sensed reflectance into a coupled crop growth–radiative transfer model. We generated a time series of 8-day, 30-m-resolution synthetic Kalman Smoothed (KS) reflectance by combining MODIS surface reflectance products with Landsat surface reflectance using a KS algorithm. We evaluated the assimilation performance using datasets with different spatial and temporal scales (e.g., three dates for the 30-m Landsat reflectance, 8-day and 1-km MODIS surface reflectance, and 8-day and 30-m synthetic KS reflectance) into the coupled WOFOST–PROSAIL model. Then we constructed a four-dimensional variational data assimilation (4DVar) cost function to account for differences between the observed and simulated reflectance. We used the shuffled complex evolution–University of Arizona (SCE-UA) algorithm to minimize the 4DVar cost function and optimize important input parameters of the coupled model. The optimized parameters were used to drive WOFOST and estimate county-level winter wheat yield in a region of China. By assimilating the synthetic KS reflectance data, we achieved the most accurate yield estimates (R^2 = 0.44, 0.39, and 0.30; RMSE = 598, 1288, and 595 kg/ha for 2009, 2013, and 2014, respectively), followed by Landsat reflectance (R^2 = 0.21, 0.22, and 0.33; RMSE = 915, 1422, and 637 kg/ha for 2009, 2013, and 2014, respectively) and MODIS reflectance (R^2 = 0.49, 0.05, and 0.22; RMSE =1136, 1468, and 700 kg/ha for 2009, 2013, and 2014, respectively) at the county level. Thus, our method improves the reliability of regional-scale crop yield estimates.

Keywords:

WOFOST; PROSAIL; canopy reflectance; data assimilation; winter wheat yield estimation

1. Introduction

Regional-scale monitoring of crop growth, yield estimation, and forecasting are essential to design informed regional and national agricultural policies, and for commercial or planning purposes. Assimilating remote sensing information into crop growth models has been demonstrated as an effective approach for estimating or forecasting crop yield at regional scales (Dente et al., 2008; de Wit et al., 2012; Ma et al., 2013a, 2013b; Huang et al., 2015a, 2015b, 2016; Zhang et al., 2016).

Process-oriented crop growth models are powerful tools to simulate the physiological development, growth, and yield of a given crop. However, crop models do not simulate the crop canopy reflectance which is the main observation of satellite remote sensing (van Diepen et al., 1989). Although radiative-transfer models (RTMs) such as PROSAIL or the A two-layer Canopy Reflectance Model (ACRM) can simulate the spectral and bidirectional reflectance of the crop canopy (Jacquemoud et al., 2009; Kuusk, 2001), they cannot simulate crop growth, water balance, or nutrient dynamics processes. A data-assimilation scheme aims to provide optimal merging of observations, models, and prior knowledge in order to obtain the best possible estimate of the state of a system. Modeling frameworks that couple crop models with RTMs result in more comprehensive modeling of temporal changes in the crop canopy’s spectral reflectance response and in the underlying crop, water, and nutrient processes (Ma et al., 2008; Thorp et al., 2012; Wu et al., 2013; Zhou et al., 2017). Thus, the assimilation of remote sensing reflectance into crop growth models has showed promise for crop yield estimates and forecasting at regional scale.

Simulation results can be constrained by RS observations by reinitialize the input parameters of the RTM and crop model. Then crop yield and other biophysical variables that cannot be directly estimated solely by RS inversion can be simulated. Rather than using high-level remotely sensed biophysical products (e.g., LAI, evapotranspiration, soil moisture), it is advantageous to directly assimilate satellite canopy-surface such as the reflected spectral radiance or albedo. From a data-assimilation perspective, this also has the obvious advantage of allowing researchers to track uncertainties in the observations, which can be far more easily characterized for satellite radiance or reflectance than for higher-level remotely sensed products such as LAI (Quaife et al., 2008).

Two main categories of data-assimilation schemes can be divided into two types in the context of crop yield estimation. The first is re-initialization or calibration, in which parameters of the crop growth model are updated based on multiple observations. LAI is widely used in this category generally, although estimates of evapotranspiration (ET) can also provide key constraints to water-use estimates. Such an approach is usually implemented through a cost function based on a variational data-assimilation strategy (Dente et al., 2008; Wang et al., 2010). The second data-assimilation category uses a sequential strategy to correct the trajectory of crop state variables (typically, LAI or soil moisture) by getting a balance between the model's expectation and observations (Qin et al., 2009; Ines et al., 2013).

A number of researchers have used LAI as a direct driver of the model (e.g., Fang et al., 2011) or have directly assimilated the LAI product into the model (Dente et al., 2008; de Wit et al., 2012; Huang et al., 2015b, 2016). Regional remotely sensed LAI products (e.g., MODIS MOD15 or CYCLOPES LAI) are usually retrieved by physically inversion based on canopy-reflectance models (Knyazikhin et al., 1998). Scale mismatch between coarse remotely sensed pixels and typical field sizes simulated by crop model is a major factor to limit the performance of agricultural data assimilation applications at a regional scale (Duveiller et al., 2013; Huang et al., 2015b, 2016).

Several previous studies found that time series of reflectance or vegetation index data could be assimilated into a coupled crop growth–RTM model to obtain successful results and avoid the process of regional LAI retrieval. Weiss et al. (2001)

coupled canopy RTM (Scattering by Arbitrarily Inclined Leaves, SAIL) and a crop growth model (STICS) to simulate reflectance time series; Launay and Guerif (2005) assimilated four to six SPOT and aerial photography datasets into the SUCROS model, which was coupled with the SAIL reflectance model; and our previous work (Ma et al., 2013b) assimilated an NDVI time series from the Chinese HJ-1 A/B satellite into the coupled WOFOST–ACRM model using an ensemble Kalman filter assimilation strategy. Besides that, there are some studies demonstrated that a successful assimilation of remote sensing observations into crop growth models requires suitable spatial and temporal resolutions data (Machwitz et al., 2014; Huang et al., 2015b). Thus, upscaling the temporal resolution of Landsat data by taking advantage of MODIS data would provide fundamental data to investigate the impacts of the optimal assimilation timing on the performance of the data assimilation.

Several approaches based on information available from other dates and sensors have been proposed to simulate medium-resolution RS data at locations and times for which observation does not exist (Gao et al., 2006; Roy et al., 2008; Zhu et al., 2010). Our previous research demonstrated the suitability of using a Kalman Smoother algorithm to generate a continuous time series of synthetic medium-resolution images for various ecosystems (Sedano et al., 2014). The Kalman smoother differs from previous approaches because it uses a state-space model framework to explicitly incorporate uncertainties in the calculation of a variable's state and provides the best unbiased linear estimate for each state (Mathieu and O'Neill, 2008). This approach can create a continuous time series of synthetic medium-resolution images of spectral indices and spectral reflectance. By accounting for uncertainties, this approach becomes suitable for regions with different data volumes, including data-scarce regions and regions where the cloud coverage reduces the number of available medium-resolution images. This approach has been successfully implemented to improve crop mapping in Western Europe with the PROBA-V satellite (Kempeneers et al., 2014) and to integrate higher-resolution remote sensing information into a crop model to estimate winter wheat yields in the Northern China Plains (Huang et al., 2016).

In the present study, we developed a data-assimilation framework that incorporates remotely sensed reflectance into a coupled WOFOST–PROSAIL model to estimate wheat yield in the North China Plain. First, we generated a continuous time series of synthetic surface reflectance images at medium spatial resolution with 30 m using a Kalman Smoother algorithm that integrates the available Landsat and MODIS imagery. Second, a four-dimensional variational data assimilation (4DVar) cost function was constructed to assimilate remote sensing and WOFOST-PROSAIL coupled model simulated reflectance using a faster but equally accurate computation of the data-assimilation algorithm at a 30-m scale. Finally, we assessed the accuracy of the winter wheat yield estimates based on official statistics using remotely sensed reflectance datasets for three different spatial and temporal scales. To demonstrate the benefits of this approach, we used reflectance data from 2009, 2013, and 2014 for an agricultural region of the North China Plain.

2. Study area

The study was conducted in a planting area dominated by winter wheat in China’s southern Hebei Province and northern Shandong Province (Figure 1). The region consists of 58 counties. The prevailing planting pattern is an intensive dual-cropping system based on winter wheat and summer crops such as corn. The region is characterized by alluvial plains, with loam soils and abundant organic matter, and its continental monsoon climate. Figure 2 contains the daily temperature and precipitation data for the three years in our study; these data suggest that 2009 and 2014 had normal climatic conditions for the study area, whereas 2013 was unusually cold and had several damaging cold weather events mid-March, mid-April, and grain-filling stage that induced subsequent production losses. Accumulated rainfall is commonly below annual evapotranspiration (300 to 500 mm) in the winter wheat growing season, and an average of 350 mm of underground water must be extracted for irrigation annually to cover the water deficiency of winter wheat. High winter wheat yields are traditionally reported from this region. Generally, winter wheat is sown at the beginning of October and harvested in early or mid-June in the following year.

[Insert Figure1 near here]

[Insert Figure2 near here]

3. Models and Data

3.1 WOFOST

The WOFOST crop-growth model (de Wit, 1965; Diepen, 1989; Boogaard et al., 2013) is a mechanistic model that simulates crop growth based on underlying processes such as photosynthesis and respiration, and how these processes are influenced by environmental conditions. WOFOST estimates LAI, aboveground biomass, and storage organ biomass (i.e., grain yield) at a daily time step for a specific crop type. The model can run in potential mode (with no limitations caused by water and nutrient stress) or in water-limited mode (with soil moisture stress). In the present study, we chose potential mode because winter wheat in the study area does not usually suffer from water stress through adequate irrigation. Ma et al. (2013b) and Huang et al. (2015b) provide details of the parameterization and calibration of WOFOST for winter wheat in the study area.

3.2 PROSAIL

PROSAIL combines the SAIL canopy reflectance model (Verhoef, 1984, 1985) with the PROSPECT leaf optical properties model (Jacquemoud and Baret, 1990; Jacquemoud et al., 1995). PROSPECT simulates leaf reflectance and transmission as a function of the chlorophyll a + b concentration (C_{ab}, μg·cm^{-2}), brown pigment content (C_{brown}, μg·cm^{-2}), leaf water content (C_w, g·cm^{-2}), dry matter content (C_m, g·cm^{-2}), and a leaf structure variable (N, unitless). SAIL is a one-dimensional bidirectional turbid-medium canopy-reflectance model, and was one of the earliest models to simulate reflectance from the top of the canopy (Verhoef, 1984, 1985). The model has been improved to consider the hot-spot effect (Kuusk, 1991). The model's inputs are LAI (m^2·m^{-2}), two leaf-inclination distribution-function parameters (LIDFa and LIDFb, which vary with the leaf distribution), a hot-spot parameter (hot, unitless), the fraction of diffuse incoming solar radiation (skyl, unitless), a dry/wet soil factor parameter (psoil, unitless), a soil brightness factor (rsoil, unitless), a sun zenith angle (tts, °), an observer zenith angle (tto, °), and a relative azimuth angle (psi, °) between the observer and the sun (Jacquemoud et al., 2009). The coupling of the two models is done through the leaf reflectance and transmittance values output by PROSPECT, which are used as inputs to SAIL for simulation of the whole bidirectional canopy reflectance.

3.3 Field data

We selected 29 sample plots that represented a range of winter wheat growing conditions throughout the study area, and monitored them from March to June 2009, during the main winter wheat growing season. Sample fields are chosen respectively from typical wheat planting parcels that are no less than 500×500 m^2 large; crop growth in these filed parcels should be representative. Five square sample subplots are taken from each sample field, measuring 100 m on each side, and crop in each subplot must be homogenous. Within these subplots in 100 m sizes, five 1-m sample plots are chosen randomly, and then the location of each test site was recorded and in situ measurements were obtained, such as the chlorophyll content (Cab), leaf water content, LAI, key phenological dates, dry matter production, and grain yield. LAI was measured using a LAI-2000 Plant Canopy Analyzer (LI-COR Inc., Lincoln, NE, USA) during seven key phenological stages: green-up, jointing, elongation, booting, heading, anthesis, and grain-filling. Field measurements of winter wheat yields were obtained by weighing the grain after harvesting in mid-June. Finally, calculating median of crop variable of a particular sample fields and recording its location. Detailed crop management was also surveyed by interviews, including the emergency dates and harvest date, planting density, irrigation dates and depth, fertilizing date and volume, and other information. Official government statistics on winter wheat yields at a county level were obtained from the 2009, 2013, and 2014 statistical yearbooks for Hebei Province (Office of People's Government of Hebei Province 2010, 2014, 2015) and Shandong Province (Statistics Bureau of Dezhou 2010, 2014, 2015, Statistics Bureau of Liaocheng 2010, 2014, 2015,).

3.4 Remote sensing data

We compiled a dataset of cloud-free (less than 10% cloud coverage) Landsat 5 TM and Landsat 8 OLI surface reflectance images. The images were acquired during the winter wheat growing seasons of 2009, 2013, and 2014, and the study area was covered by two Landsat scenes (P123R033 and P123R034). Table 1 presents an overview of Landsat images we assimilated and their corresponding growth stages, in addition, we do use more images out of growing season for the KS synthetic algorithms to constraint the synthetic reflectance curves (5, 6, 8 extra images were used in 2009, 2013, 2014 respectively). All images were obtained from the United States Geological Survey (USGS) Center for Earth Resources Observation and Science (http://earthexplorer.usgs.gov).

We also obtained MODIS surface reflectance products for the study area (MOD09A1). MOD09A1 represents the best possible observation during an 8-day period for MODIS bands 1 to 7 at 500-m resolution. We acquired two MODIS tiles (h26v05 and h27v05) form NASA Reverb (https://reverb.echo.nasa.gov) to cover the study area during all three years of our Landsat dataset. Each MODIS image was projected into the UTM/WGS84 coordinate system, and was then resampled to 30-m spatial resolution using the nearest-neighbor method to match the Landsat pixel size for use in the retrieval of a continuous time series of synthetic Landsat surface reflectance images. We established 50 ground control points distributed equally throughout the study area to ensure precise co-registration and reprojection of the MODIS and Landsat datasets. Besides that, we used the "China Meteorological Forcing Dataset" (He and Yang, 2011; Chen et al., 2011) as our weather driver data, this dataset contains six weather variables (temperate, pressure, humidity, wind speed, precipitation rate and download shortwave/longwave radiation) with temporal resolution of 3-hr, on a 0.1° x 0.1° grid.

[Insert Table 1 near here]

4. Data assimilation

4.1 Continuous time series of medium-resolution synthetic reflectance images using a Kalman Smoother

Reflectance information at the key phenological stages is crucial for crop monitoring and for yield estimation and forecasting. We implemented a Kalman Smoother algorithm to generate a time series of synthetic surface reflectance images at medium spatial resolution (30 m) based on the available Landsat and MODIS imagery for the study area. The Kalman Smoother algorithm is a state-space statistical model that combines observations, model estimations, and their respective uncertainties in a recursive manner to estimate the state of a process while minimizing the error (Kalman, 1960; Welch and Bishop, 2006). This approach uses the available Landsat surface reflectance images as observations and the available MODIS surface reflectance images as the source of a transition model that defines crop phenology. Sedano et al. (2014) provide a detailed description of the implementation. We used a crop type mask to stratify the analysis into different categories of coverage by winter wheat (40 to 60%, 60 to 80%, and 80 to 100%) and define specific transition models for areas with different crop cover percentages.

4.2 Coupling the WOFOST and PROSAIL models

Unlike when LAI is assimilated into a process-based dynamic model to obtain crop yield estimates, assimilating remotely sensed reflectance into a crop growth model requires linking the crop growth model with an RTM (e.g., PROSAIL, ACRM) to simulate the effects of the daily reflectance in the visible, NIR, and SWIR parts of the spectrum during the growing season. This is done through the LAI simulated by the crop model, which is used as input for the RTM along with other biophysical or biochemical parameters (Fang et al., 2011; Ma et al., 2013b; Wu et al., 2013).

WOFOST simulates daily LAI when the meteorological, soil, and crop input parameters are specified. In this study we used the WOFOST-simulated LAI as the input parameter for PROSAIL to calculate the daily spectral reflectance for the wavelength range from 400 to 2500 nm. Both models were coupled through the LAI state variable using a program written in FORTRAN.

In addition, we generated C_{ab} through a piecewise linear interpolation method based on field data for three key periods (booting, heading, and grain-filling) as inputs.

We determined the leaf structure parameter N based on an empirical relationship with specific leaf area (SLA) developed by Jacquemoud and Baret (1990). The C_m values were given through empirical relationship with dry matter of leaves simulated by WOFOST, the LIDFa parameter was given an initial value of 0.8 and re-initialized by the 4DVar data-assimilation, and LIDFb was set as a fixed value of 0. The view zenith angle was obtained from the Landsat metadata and the solar zenith angle was calculated from the longitude and overpass time in the Landsat metadata. The time series of psoil (the dry/wet soil factor) was determined through an empirical relationship with daily precipitation; in this relationship, we set psoil to 0 after an effective rainfall (i.e., more than 3 mm of rain), then added 0.1 to the parameter each day until the next effective rainfall event. We set rsoil (the soil brightness factor), C_w to a fixed value during winter wheat growing season.

[Insert Table 2 near here]

4.3 Assimilation of remotely sensed reflectance into WOFOST–PROSAIL using the 4DVar algorithm

Minimization of cost function of four-dimensional variational (4DVAR) was conducted to derive a new set of input parameters (re-initialized parameters) that will be an input for the WOFOST-based yield estimate. The selection of re-initialization parameters is crucial in a 4DVar assimilation strategy (de Wit et al., 2012; Huang et al., 2015b). Only the parameters that most strongly affect LAI and yield are selected for the re-initialization; however, the correlations among the parameters and the physical meaning of the re-initialized parameters must be accounted for. One particular parameter, the sum of the effective temperatures from emergence to anthesis (TSUM1), has been shown by previous sensitivity analyses to be key WOFOST parameters for grain and biomass yield estimates (Ma et al., 2013a). Also, the total initial dry weight of the crop (TDWI) greatly influences the rate of increase of the crop LAI and affects the maximum LAI that to be reached during the growing season (de Wit et al., 2012; Huang et al., 2015b). While WOFOST does not include a crop planting-density parameter, planting density strongly influences the subsequent biomass and yield. TDWI can represent a proxy for the crop planting density because TDWI reflects the actual biomass that generates subsequent growth. The SPAN parameter represents the lifespan (in days) of leaves growing at 35°C. Thus, SPAN determines the rate and timing of leaf senescence, and therefore determines the time when LAI begins to decrease after heading (Curnel et al., 2011, Huang et al., 2015b). The WOFOST-simulated LAI values are sensitive to TSUM1, TDWI, and SPAN, subsequently it greatly influences reflection in the visible, NIR, and SWIR wavelengths (Figure 3a-c). In addition, leaf inclination distribution in SAIL model was presented by two parameters, LIDFa controls the average leaf inclination angle while LIDFb affects the bimodality (Verhoef, 1998). For simplicity and efficiency, we set LIDFb equal to 0. We found that LIDFa can strongly influences spectral reflectance in the red, NIR, and SWIR bands (Figure 3d), but it varies with crop's development. For winter wheat, it was erectophile at beginning and turn to planophile at maturity (Duan et al., 2016). Thus, we applied a linear interpolation between the two stages to obtain a LIDF parameter series along with DVS. Simultaneously, we reinitialized TSUM1, TDWI, SPAN, and LIDFa at the grain-filling stage (DVS=1.3, at filling stage) for winter wheat pixels in this variational assimilation procedure.

[Insert Figure 3 near here]

Figure 4 shows the flowchart for the process of assimilating remotely sensed reflectance into the coupled model to estimate the winter wheat yield. The WOFOST-PROSAIL coupled model was considered as a dynamic-process model. The LAI simulated by WOFOST were used as input for the PROSAIL model in the retrieval of spectral reflectance at red, NIR and SWIR wavelengths. The 4DVar data assimilation procedure integrates remotely sensed reflectance (observations) and modeled reflectance from coupled WOFOST-PROSAIL model. Four parameters, including TSUM1, TDWI and SPAN, LIDFa (DVS=1.3, at filling stage) were re-initialized through the minimization of 4DVar cost function. The 4DVar cost function in this study, $J(x)$, was constructed as follows:

$$J(x) = (\mathbf{X}-\mathbf{X}^{\mathbf{b}})^{\mathrm{T}}\mathbf{B}^{-1}(\mathbf{X}-\mathbf{X}^{\mathbf{b}}) + \frac{c}{T}\sum_{t=1}^{T}[\mathbf{Y}_t-\mathbf{H}_t(\mathbf{X})]^{T}\mathbf{Q}^{-1}[\mathbf{Y}_t-\mathbf{H}_t(\mathbf{X})] \quad (1)$$

where **X** represents the vector of reinitialized parameters (TSUM1, TDWI, SPAN, LIDFa); $\mathbf{X}^{b}$ represents the *prior* knowledge on these four parameters; **B** is the error covariance matrix for the four parameters; T represents the set of observation times; $\mathbf{Y}_t$ represents the remotely sensed reflectance vector for the specific red, NIR, and SWIR wavelengths on observation date t; $\mathbf{H}_t$ represents the observation operator namely the coupled WOFOST–PROSAIL model, **X** is model's inputs parameters, and it's outputs are reflectance; c is a constant value to balance the impact of the observations in the assimilation procedure; and **Q** represents the observation error covariance matrix at different wavelengths. In the present study, we used constant values for the observational errors at different times: 0.05, 0.03, and 0.04 for the red, NIR, and SWIR wavelengths, respectively. B was defined through Markov Chain Monte Carlo approach based on Bayesian theory (Toshichika et al., 2009).

[Insert Figure 4 near here]

To find the optimal values of the four parameters, we used the shuffled complex evolution–University of Arizona (SCE-UA) algorithm (Duan, 1994) to minimize the error between the modeled reflectance and the remotely sensed reflectance in the 4DVar cost function. The graphs in Figure 3 present the initial values for these parameters and their minimum and maximum ranges in the SCE-UA optimization algorithm. We recalibrated the four parameters of TSUM1, TDWI, LIDFa, and SPAN using the 4DVar assimilation procedure and used these values as the new inputs for WOFOST to estimate the winter wheat yield for each cell in the grid.

4.4 Assimilation of the 30-m-resolution data

There are totally 12.77×10^6 30-m grid cells within our study area, it would make the computation unacceptable slow if we conduct assimilation on every 30-m cell size. We developed a “grid and cluster” strategy based on the canopy reflectance profile so that the data assimilation would be conducted only for each pixel category. Figure 5 shows that the grid and cluster strategy included three steps: In the first step, we stacked the 30-m-resolution time series of TM/OLI and KS synthetic reflectance values during winter wheat growing season, and clipped it into 10-km grid cells. In the second step, we conduct ISODATA clustering analysis (Bezdek, 1980) for the 30-m-resolution time series of reflectance values during the growing season. Each 10-km cell in the grid was classified into up to approximately 40 cluster categories, with the number of categories calculated by dividing the number of pixels by 20, and with a maximum of 40 categories. Then each cluster category was assigned the mean reflectance value of all the pixels in this category. In the third step, we ran the data-assimilation algorithm for all the clusters in all cells of the grid, thereby obtaining an assimilated yield table for every cluster category within each 10-km cell of the grid. Finally, we regenerated the spatial yield map using the assimilated yield table and the clustering analysis map, thereby obtaining the spatial pattern of yield at a 30-m spatial resolution. In this study, we assimilated two 30-m reflectance datasets (i.e., the Landsat reflectance and the synthetic KS reflectance) into WOFOST–PROSAIL using the 4DVar algorithm.

[Insert Figure 5 near here]

The right part of Figure 5 shows an example of the reflectance spectrum for all

30-m pixels within a typical 10-km cell. The colors of the spectrum profiles represent the cluster categories, and each profile represents a stack of the reflectance values in three wavelength bands (red, NIR, and SWIR) on 15 observation dates that cover the entire growing season. In total, the 10-km grid cell in Figure 5 contains 60,100 30-m pixels, which we classified into 40 clusters; the mean reflectance in the red, NIR, and SWIR for the 30-m pixels ranged from 0.03 to 0.48. The average value for a cluster category can substitute for the observation to be assimilated into coupled WOFOST–PROSAIL model. Higher dispersion of reflectance curves from DOY 160 to 176 was observed due to the difference of harvest of winter wheat and the sowing of summer maize.

5. Results

5.1 Synthetic reflectance using the Landsat and MODIS reflectance

We produced a continuous time series of surface reflectance (red, NIR, and SWIR) values at a 30-m spatial resolution and an 8-day time step for three years (2009, 2013, and 2014) using two Landsat images. The synthetic KS reflectance improved the temporal resolution of the Landsat data during the winter wheat growing season. We then used the continuous time series of synthetic reflectance values at 30-m resolution as inputs for the 4DVar cost function.

Figures 6 show the resulting evolution of NIR surface reflectance during the winter wheat growth cycle (DOY 68 to 164), using the 2013 data as an example. Overall, the synthetic time series of surface reflectance generally captured the temporal dynamics of the winter wheat phenological cycle while retaining the spatial detail of the Landsat images. The spatial detail in these images is sufficient to reveal the locations of population centers, main roads, and individual fields, and reveals the variation in surface reflectance between fields and how these differences change over time. Given the mismatch between field size and the MODIS resolution, this level of detail is not visible in the MODIS sequence, where the reflectance of each pixel results from the contribution of many fields.

[Insert Figure 6 near here]

Figure 7 shows the temporal evolution of the synthetic KS, Landsat, and MODIS reflectance data for a representative pixel, using data from 2013 as an example. The red and SWIR curves present similar patterns, with minima during the peaks of the winter wheat and maize cycles and a maximum after the winter wheat harvest. The NIR curve presents a peak between DOY 120 and 140 that corresponds to the heading stage of winter wheat, followed by a decline around DOY 160 to 180 during the harvest, followed by a second cultivation cycle of the summer maize. The lower spatial resolution of the MODIS surface reflectance results in smoother temporal profiles, whereas the synthetic KS reflectance shows larger temporal variations in reflectance for a given pixel during the growing season. The uncertainties of the KS were lowest (zero) when Landsat observations existed, but the uncertainty increased as the number of time steps without a Landsat observation increased, highlighting the importance of frequent Landsat observations to obtain accurate estimates.

[Insert Figure 7 near here]

5.2 Simulated reflectance using WOFOST–PROSAIL model

WOFOST–PROSAIL generated reflectance from the initial WOFOST-simulated LAI inputs. Figure 8 compares these simulated reflectance values to the MODIS 500-m reflectance product (MOD09A1) for seven wavelength bands. We observed similar trends for the temporal evolution of the WOFOST–PROSAIL simulations and the MODIS reflectance, but there were discrepancies in the amplitudes of the variations. Reflectance in the NIR region increased rapidly during the winter wheat growth due to the increasing amount of green leafy vegetation, but decreased in the visible region, including red, green, and blue wavelengths. For the SWIR region, which is sensitive to the leaf water content, the maximum values correspond to the start of grain-filling stage.

A large lag between the observed and modeled reflectance was observed in the post-heading period for the MODIS Bands 5 and 6 (0.21 and 0.08, respectively, on average; Figure 8). This can be explained by the difficulty of accurately specifying how the C_w values vary with phenology during winter wheat growing season. We observed systematic underestimation in the red (620-670 nm) and blue (459-479 nm) bands. A possible reason may be that the characteristics of the reflectance depend on phenology for several key inputs of PROSAIL (e.g., soil reflectance, N, C_w) was not accurately given the values. Another potential reason is that PROSAIL assumes the simulated units as pure planting areas, but most of the 30-m Landsat pixels represent a mixture of crops and of other land uses; thus, other components of the image would influence the signal perceived by the sensors.

[Insert Figure 8 near here]

5.3 Assimilation of the three reflectance datasets into WOFOST–PROSAIL at the field scale

We assessed the accuracy of the assimilated yield in comparison with field-measured yields from the 29 sample plots at the field scale. Table 3 compares the estimated yield with field-measured data for the three spatial and temporal resolutions in the reflectance datasets. We achieved the best accuracy by assimilating the synthetic KS reflectance into WOFOST–PROSAIL, with the highest R^2 (0.52) and lowest RMSE (710 kg ha^{-1}). This can be explained because the synthetic KS reflectance increases the amount of temporal information at key stages of the growing season with respect to the Landsat images and improves the spatial details with respect to the MODIS dataset. Assimilation of the Landsat reflectance achieved the second-highest accuracy, with R^2 = 0.38 and RMSE = 762 kg/ha. Assimilating the time series from the MODIS reflectance achieved a lower accuracy, with R^2 = 0.25 and RMSE = 803 kg/ha. The WOFOST-simulated yields without data assimilation achieved the lowest accuracy, with R^2 = 0.15 and RMSE = 808 kg/ha.

[Insert Table 3 near here]

5.4 Assimilation of the three reflectance datasets into WOFOST–PROSAIL at a regional scale

We assimilated three remote sensing-based reflectance data with different spatial and temporal resolutions (1 km and 8-day for the MODIS data, 30 m for the Landsat TM/OLI data, and 30 m and 8-day for the KS synthetic reflectance) from 2009, 2013, and 2014 into WOFOST–PROSAIL using the 4DVar assimilation algorithm. Figure 9 compares the mapped WOFOST-simulated yield for each dataset and year. The WOFOST simulation without assimilation was applied at a 10-km grid size, which is the same as the meteorological datasets. On the other hand, 1-km MODIS pixels with at least 60% winter wheat pixel purity was assimilated, and 30-m Landsat reflectance and KS synthetic data were assimilated by the “grid and cluster” strategy.

[Insert Figure 9 near here]

In the government statistics, yields are compiled at a county level. To allow a comparison with these statistics, we aggregated the assimilated yield pixels or clusters at a county level for the 58 counties in the study area so that the results could be validated. Figure 10 shows the resulting scatterplots for the simulated yields and government statistics. The results indicated that WOFOST is not capable of capturing the dynamic range in the regional statistics. However, the data assimilation is more successful in reducing bias then representing the spatial variability. The region-wide mean wheat yield averaged 6089, 6609, and 6659 kg ha^{-1} in 2009, 2013 and 2014 respectively, and 95% of the yield was in the range of 4000 to 8000 kg ha^{-1}. The yields without assimilation had a low coefficient of determination and large error (R^2

= 0.14, 0.06, and 0.10 and RMSE = 1002, 1586, and 1315 kg ha^{-1} for 2009, 2013, and 2014 respectively). Although the WOFOST simulation without data assimilation captured some of the spatial variability of wheat yield (Figure 9), it generally overestimated wheat yields except in 2013 (6398, 4780, 7502 kg ha^{-1} on average in 2009, 2013 and 2014 respectively).

[Insert Figure 10 near here]

The 1-km and 8-d MODIS reflectance time series from green-up (about DOY 60) to maturity (about DOY 160) was directly assimilated into WOFOST–PROSAIL using the 4DVar assimilation strategy (Figure 10). The assimilation results indicated low accuracy, with R^2 = 0.49, 0.05, and 0.22 and RMSE = 1136, 1468, and 700 kg ha^{-1} for 2009, 2013, and 2014, respectively.

Direct assimilation of the 30-m Landsat TM/OLI reflectance data captured more of the spatial variability of winter wheat yields throughout the study area because of the high spatial resolution (Figure 9c). Its yield simulation accuracy was also higher than that of the MODIS data, with R^2 = 0.21, 0.22, and 0.33 and RMSE = 915, 1422, and 637 kg ha^{-1} for 2009, 2013, and 2014, respectively. Comparison of the results from the three years shows that the assimilation at two key growth stage (heading, grain-filling) achieves better results, but due to the impact of the 16-day Landsat revisit frequency, it is difficult to obtain the required key information during the growing season.

The estimated yields from assimilation of the synthetic KS reflectance dataset from DOY 60 to maturity, with 30-m resolution and an 8-day interval, agreed well with the spatial pattern of the official statistical yields at the county level (Figure 9d). Overall, the assimilation of the KS synthetic reflectance dataset took advantage of the benefits of the MODIS MOD09A1 and Landsat TM/OLI data, and maintained a good balance between improving correlation and low error, with R^2 = 0.44, 0.39, and 0.30 and RMSE = 598, 1288, and 595 kg ha^{-1} for 2009, 2013, and 2014, respectively. This can be explained by the higher temporal and spatial resolution of the synthetic KS reflectance series, which resulted from integration of the MODIS reflectance time series with the more accurate Landsat TM/OLI reflectance values.

6. Discussion

In this study, we have developed a data-assimilation framework to incorporate high resolution reflectance data into a coupled crop growth and canopy radiative transfer model (WOFOST–PROSAIL). The coupling of the reflectance observations within the assimilation scheme has obvious advantages, as it accounts for the propagation of uncertainty through the mapping from reflectance data to the state variable (LAI), and can directly incorporate observations from different sensors in a consistent and coherent fashion. However, this strategy requires an accurate calibration of key parameters in the coupled crop–RTM model, particularly when the data-assimilation practices extend to a regional scale.

Determining the optimal values for free parameters is a time-consuming process for large datasets. Thus, improving the computational efficiency is crucial for use of our method for data assimilation in large regions and in high spatial resolutions. We developed a grid and cluster method to solve the problem of long computation times and improve the efficiency of the data assimilation calculations. The grid and cluster strategy developed in the present study was generally successful and enabled us to conduct the assimilation scheme at a large scale with 30-m resolution. It illustrates that full coupling of the RTM within a data-assimilation system would become possible, improving biophysical and biochemical monitoring of crops. Besides of that, new technological breakthroughs such as the use of machine-learning approaches

(Lewis et al., 2012; Gómez-Dans et al. 2016) can be used to represent the input–output relationships of RTMs would greatly accelerate performance, we are planning to address this in a future study.

In this study, we generated Kalman Smoothed reflectance with 30-m and 16-d resolution, it's actually a both temporally and spatially upscaled dataset. The comparison between assimilating KS reflectance and MOD09 indicates that assimilating spatially upscaled reflectance result in accuracy improvement (lower RMSE) and similar precision (R^2). Meanwhile, the comparison between assimilating KS reflectance and TM/OLI illustrates that assimilating temporally upscaled reflectance could improve assimilation accuracy and precision both.

A low temperature caused frost damage in 2013 and significantly affected the performance of data assimilation. This indicates that WOFOST requires further calibration to account for the effect of low temperature on dry matter accumulation during subsequent growth periods. When frost damage occurs, several important crop parameters (e.g., the leaf CO_2 assimilation rate, conversion efficiency of assimilates, and partitioning parameters) would change for the following growth period. Thus, taking into account temporal variability of these parameters are crucial for improve the simulation of growth process.

We conducted data assimilation for three years, the perfect evaluating the performance of data assimilation should be performed both at the field and regional scales. Due to the lack of enough field data in 2013 and 2014, we only validated the data assimilation results at the county level for 2013 and 2014. We also conducted data assimilation in 2009 with the same method and scheme because we have plenty of field survey data in this year for validation. In future work, adequate field data are needed to validate the performance of data assimilation under the under extreme weather conditions (such as low and high temperatures).

The frequency of remote sensing observations has an obvious effect on the assimilation accuracy: the more reflectance observations that can be obtained during highly sensitive growth periods (from heading to flowering), the better the assimilation results. However, there’s a tradeoff between high spatial resolution and high temporal resolution: the assimilation of data with high spatial resolution is more accurate and provides more detail on spatial variation, but it requires observations that are often unavailable during the key growth periods; in contrast, yield estimation by assimilating data with high frequency results in a high correlation with official yield statistics, but it is unsuitable in actual application because few pure pixels exist in the relatively coarse-spatial-resolution data. The synthetic Kalman filter reflectance generated by the MODIS and Landsat datasets combines the advantages of high spatial resolution and high frequency; as a result, our assimilation experiments showed that the synthetic product is more stable in different years and in large region and more effective than relying on only one of the two datasets. In addition, the reflectance data (with similar spatial resolution) from different sources are easier to compare, making this approach suitable for assimilation of data from multiple sources. In addition, with time series of Sentinel 2A/2B available, these data can be assimilated to ensure sufficient frequency and spatial detail, and the reliance on synthetic reflectance images will be reduced.

The parameterization of a coupled growth – RTM model in which several key parameters vary during the crop growth period represents a challenging problem. In previous researches, we used LAI as the state variable, and assimilated the adjusted LAI into the WOFOST model to significantly reduce the RMSE for the estimated winter wheat yields using the 4DVar assimilation algorithm (Huang et al., 2015b) and an ensemble Kalman filter algorithm (Huang et al., 2016). In the present study, we instead assimilated the remotely sensed reflectance data from red, NIR, and SWIR wavelengths into the coupled crop growth and radiative transfer model. Another challenge for our previous approaches is that large amounts of high-quality ancillary data are required to generate the scale-adjusted LAI or KF synthetic LAI over a regional scale (Huang et al., 2015b, 2016). The present approach integrates the more direct remotely sensed observational reflectance signals into the coupled crop and RTM model, thereby avoiding the need for LAI retrieval and reducing the requirement for high-quality ancillary data over a regional scale. Thus, assimilating reflectance data appears to be a more promising approach for operational monitoring and forecasting of regional crop yield. At a regional scale, both strategies improved the estimation accuracy for winter wheat yield compared with running WOFOST without data assimilation. In the previous research, accuracy of yield estimation by assimilating LAI with 4DVar (R^2 = 0.48; RMSE = 151.92 kg ha^{-1}) and with an ensemble Kalman filter (R^2 = 0.43; RMSE = 439 kg ha^{-1}) achieved slightly higher accuracy than assimilating reflectance in the present study (R^2 = 0.44, RMSE = 598 kg ha^{-1}) in 2009. By assimilating the Landsat and KS synthetic data using the grid and cluster strategy, we retained the same level of spatial detail while greatly improving the computational efficiency.

In previous studies, grain yield RRMSE values at field scale were between 18 and 24% based on assimilating LAI and canopy cover data at a 30-m resolution (Silvestro et al., 2017), and some research reported RRMSE less than 10% at a field scale by assimilating 30-m-resolution vegetation indices (Zhang et al., 2016). Our results indicated that the number and distribution over the year of the Landsat images is important to capture the dynamics of the crop cycle and thus achieve a precise yield estimation. Thus, the number and acquisition dates of the Landsat images in different years and different scenes will result in variations in the accuracy of yield estimates, as it can be observed by the larger RRMSE obtained for year 2013, as we did not have any Landsat images before DOY 132 in P123R033. Integrating images from multiple sensors into this framework will ensure key periods of crop development are captured and increase the robustness of yield estimations. Working over a larger temporal and spatial domain than previous studies, our results demonstrate the effectiveness of assimilating reflectance values instead of biophysical variables or remote sensing vegetation indices and the feasibility to operate over large regions, which is a crucial consideration for practical application of this approach.

Larger spatial extents and multiple-year analysis are required to validate the robustness of data-assimilation approaches and determine how well they account for the spatial and inter-annual variability in crop yield estimates (Claverie et al., 2012; de Wit et al., 2012). Variables such as the choice of cultivars, the weather conditions, and the management decisions often change between years, and introduce uncertainties into yield estimates. There are a few studies of the variations of assimilation performance during multiple years (e.g., de Wit et al., 2012). In the present study, we conducted data assimilation for three years and the performance differs in each year, it suggests that some of the biotic or abiotic processes are probably not covered in the model, so further work need to focus on the calibration of the effects of weather conditions (such as low and high temperatures) and some other method like sequential assimilation may need to be considered. Experiments over longer periods, such as a decade, are worth to conduct to reveal the key factors that control the accuracy of the assimilation scheme.

7. Conclusions

In this study, we used the coupled WOFOST–PROSAIL model to estimate winter wheat yield at a regional level and enhanced the model's simulation accuracy by assimilating remotely sensed Landsat, MODIS, and synthetic KS surface reflectance values using the 4DVar cost function combined with the SCE-UA optimization algorithm. Assimilation of the Landsat reflectance data improved the results by providing higher-resolution data during key growth stages, whereas assimilation of the MODIS reflectance data improved the frequency of the observations; combining these two advantages using the synthetic KS approach further improved the results. Our results showed that the current 1-km MODIS surface reflectance products are not suitable for assimilation into the WOFOST–PROSAIL model because despite the relatively high R^2 achieved with this data, the RMSE was relatively large. The proposed grid and cluster strategy, a data-assimilation algorithm at a 30-m scale, produced wheat yield estimates that retained fine spatial detail while improving the computational efficiency. Our validation results showed that assimilating the time series of synthetic KS surface reflectance values improved the estimates of wheat yield at both individual-field and regional (county-level) scales. These results indicated that our new method, based on the 4DVar strategy and synthetic reflectance data, is a promising way to estimate winter wheat yield at a regional scale in the North China Plains, and may be adaptable to improve crop yield estimation in other agricultural regions of the world.

Acknowledgments

This study was supported by the National Natural Science Foundation of China (Project No. 41671418, 61661136006), and Science and Technology Facilities Council of UK- Newton Agritech Programme (Sentinels of Wheat) .We thank the journal's editors and anonymous reviewers for their efforts to improve the quality of this paper.

References

Bezdek, J. C., 1980. A convergence theorem for the fuzzy ISODATA clustering algorithms. IEEE Transactions on Pattern Analysis and Machine Intelligence, 1980(1), 1-8.

Boogaard, H., Wolf, J., Supit, I., Niemeyer, S., & van Ittersum, M. (2013). A regional implementation of WOFOST for calculating yield gaps of autumn-sown wheat across the European Union. Field Crops Research, 143, 130-142.

Chen, Y. Y., K. Yang, J. He, J. Qin, J-C Shi, J-Y Du, Q. He, 2011. Improving land surface temperature modeling for dry land of China. J. Geophys. Res., 116, D20104

Claverie, M., Demarez, V., Duchemin, B., Hagolle, O., Ducrot, D., Marais-Sicre, C., et al., 2012. Maize and sunflower biomass estimation in southwest France using high spatial and temporal resolution remote sensing data. Remote Sens. Environ., 124, 844-857.Curnel, Y., de Wit, A.J.W., Duveiller, G., Defourny, P., 2011. Potential performances of remotely sensed LAI assimilation in WOFOST model based on an OSS experiment. Agric. For. Meteorol. 151(12), 1843-1855.

Dente, L., Satalino, G., Mattia, F., Rinaldi, M., 2008. Assimilation of leaf area index derived from ASAR and MERIS data into CERES–Wheat model to map wheat yield. Remote Sens. Environ. 112(4), 1395–1407.

de Wit C.T., 1965. Photosynthesis of leaf canopies. Agricultural Research Report 663, Pudoc: Wageningen. 1-57.

de Wit, A., Duveiller, G., Defourny, P., 2012. Estimating regional winter wheat yield with WOFOST through the assimilation of green area index retrieved from MODIS observations. Agric. For. Meteorol., 164, 39-52.

Diepen, C.V., Wolf, J., Keulen, H.V. and Rappoldt, C., 1989. WOFOST: a simulation model of crop production. Soil Use and Management, 5(1), pp.16-24.

Duan, Q.Y., Sorooshian, S. and Gupta, V.K. 1994. Optimal use of the SCE-UA global optimization method for calibrating watershed models. Journal of Hydrology 158.3-4: 265-284.

Duan, T., Chapman, S.C., Holland, E., Rebetzke, G.J., Guo, Y. and Zheng, B., 2016. Dynamic quantification of canopy structure to characterize early plant vigour in wheat genotypes. Journal of Experimental Botany, 67(15), pp.4523-4534.

Duveiller, G., Baret, F. and Defourny, P., 2013. Using thermal time and pixel purity for enhancing biophysical variable time series: an interproduct comparison. IEEE Transactions on Geoscience and Remote Sensing, 51(4), pp.2119-2127.

Fang, H.L., Liang, S.L., Hoogenboom, G., 2011. Integration of MODIS LAI and vegetation index products with the CSM-CERES-Maize model for corn yield estimation. Internat. J. Remote Sens. 32(4), 1039-1065.

Gao, F., Masek, J., Schwaller, M., Hall, F. 2006. On the blending of the Landsat and MODIS surface reflectance: predicting daily Landsat surface reflectance. IEEE Trans. Geosci. Remote Sens., 44(8), 2207-2218.

Gómez-Dans, J.L., Lewis, P.E. and Disney, M., 2016. Efficient emulation of radiative transfer codes using Gaussian processes and application to land surface parameter inferences. Remote Sensing, *8*(2), 119.

He, J., Yang K., 2011. China Meteorological Forcing Dataset. Cold and Arid Regions Science Data Center at Lanzhou. doi:10.3972/westdc.002.2014.db

Huang, C., Li, X., Lu, L. and Gu, J., 2008. Experiments of one-dimensional soil moisture assimilation system based on ensemble Kalman filter. Remote Sens. Environ., 112(3), 888-900.

Huang, J., Ma, H., Su, W., Zhang, X., Huang, Y., Fan, J., Wu, W., 2015a. Jointly assimilating MODIS LAI and ET products into the SWAP model for winter wheat yield estimation. IEEE J. Sel. Topics Appl. Earth Observ. Rem. Sens., 8(8), 4060-4071.

Huang, J., Sedano, F., Huang, Y., Ma, H., Li, X., Liang, S., Tian, L., Zhang, X., Fan, J. and Wu, W., 2016. Assimilating a synthetic Kalman filter leaf area index series into the WOFOST model to improve regional winter wheat yield estimation. Agric. For. Meteorol., 216, 188-202.

Huang, J., Tian, L., Liang, S., Becker-Reshef, I., Su, W., Zhang, X., Zhu, D., Wu, W., 2015b. Improving winter wheat yield estimation by assimilation of the leaf area index from Landsat TM and MODIS data into the WOFOST model. Agric. For. Meteorol., 204, 106-121.

Ines, A. V., Das, N. N., Hansen, J. W., & Njoku, E. G., 2013. Assimilation of remotely sensed soil moisture and vegetation with a crop simulation model for maize yield prediction. Remote Sens. Environ., 138, 149-164.

Jacquemoud, S., & Baret, F. 1990. PROSPECT: a model of leaf optical properties spectra. Remote Sens. Environ., 34, 75−91.

Jacquemoud, S., Baret, F., Andrieu, B., Danson, F. M., & Jaggard, K., 1995. Extraction of vegetation biophysical parameters by inversion of the PROSPECT+SAIL model on sugar beet canopy reflectance data—application to TM and AVIRIS sensors. Remote Sens. Environ., 52, 163−172.

Jacquemoud, S., Verhoef, W., Baret, F., Bacour, C., Zarco-Tejada, P. J., Asner, G. P., Ustin, S.L., 2009. PROSPECT + SAIL models: a review of use for vegetation characterization. Remote Sens. Environ., 113, S56–S66.

Kalman, R. E. 1960. A new approach to linear filtering and prediction problems. Trans. ASMAE–J. Basic Eng., 82(Series D), 35-45.

Kempeneers, P. Sedano, F., Piccard, I. and Eerens, H. 2014. Data Assimilation of PROBA-V 100 and 300 m, IEEE J. Sel. Topics Appl. Earth Observ. Rem. Sens., 9(7), 3314-3325.

Knyazikhin, Y., Martonchik, J.V., Myneni, R.B., Diner, D.J. and Running, S.W., 1998. Synergistic algorithm for estimating vegetation canopy leaf area index and fraction of absorbed photosynthetically active radiation from MODIS and MISR data. Journal of Geophysical Research: Atmospheres, 103(D24), 32257-32275.

Kuusk, A. 1991. The hot spot effect in plant canopy reflectance. P. 139-159 in Myneni, R.B., and Ross, J. (eds.) Photon-Vegetation Interactions, Springer, Berlin.

Kuusk, A., 2001. A two-layer canopy reflectance model. Journal of Quantitative Spectroscopy & Radiative Transfer. 71, 1–9.

Launay, M., and M. Guerif., 2005. Assimilating remote sensing data into a crop model to improve predictive performance for spatial applications. Agriculture Ecosystems & Environment, 111(1–4): 321–339.

Lewis, P., Gomez-Dans, J., Kaminski, T., Settle, J., Quaife, T., Gobron, N., Styles, J., Berger, M. (2012) An Earth observation land data assimilation system (EO-LDAS). Remote Sens. Environ., 120, 219-235.

Ma, G., Huang, J., Wu, W., Fan, J., Zou, J., Wu, S., 2013a. Assimilation of MODIS-LAI into WOFOST model for forecasting regional winter wheat yield. Math. Comp. Model., 58(3-4), 634-643.

Ma, H.Y., Huang, J.X., Zhu, D.H., Liu, J.M., Zhang, C., Su, W., Fan, J.L., 2013b. Estimating regional winter wheat yield by assimilation of time series of HJ-1 CCD into WOFOST–ACRM model. Math. Comp. Model., 58(3-4), 753-764.

Ma, Y.P., Wang, S.L., Zhang, L., How, Y.Y., Zhang, L.W., He, Y.B., Wang, F.T., 2008. Monitoring winter wheat growth in North China by combining a crop model and remote sensing data. Internat. J. Appl. Earth Observ. Geoinform., 10(4), 426–437.

Machwitz, M., Guistarini, L., Bossung, C., Frantz, D., Schlerf, M., Lilienthal, H., Wandera, L., Matgen, P., Hoffmann, L., Udelhoven, T. 2014. Enhanced biomass prediction by assimilating satellite data into a crop growth model. Environ. Model. Softw., 62, 437-453.

Mathieu, P., and O'Neill, A., 2008. Data assimilation: from photon counts to Earth system forecasts. Remote Sens. Environ., 112(4), 1258–1267.

Office of People's Government of Hebei Province, Hebei Provincial Bureau of Statistics, 2010, 2014, 2015. Major economic indicators of each county. Hebei Rural Statistical Yearbook. China Statistics Press, Beijing. (in Chinese)

Qin, J., Liang, S., Yang, K., Kaihotsu, I., Liu, R., & Koike, T., 2009. Simultaneous estimation of both soil moisture and model parameters using particle filtering method through the assimilation of microwave signal. Journal of Geophysical Research: Atmospheres, 114(D15).

Quaife, T., Lewis, P., De Kauwe, M., Williams, M., Law, B.E., Disney, M. and Bowyer, P., 2008. Assimilating canopy reflectance data into an ecosystem model with an ensemble Kalman filter. Remote Sens. Environ., 112(4), 1347-1364.

Roy, D. P., Ju, J., Lewis, P., Schaaf, C., Gao, F., Hansen, M., Lindquist, E. 2008. Multi-temporal MODIS–Landsat data fusion for relative radiometric normalization, gap filling, and prediction of Landsat data. Remote Sens. Environ., 112(6), 3112-3130.

Sedano, F., Kempeneers, P., Hurtt, G., 2014. A Kalman filter-based method to generate continuous time series of medium-resolution NDVI images. Remote Sens., 6, 12381-12408.

Silvestro, P.C., Pignatti, S., Pascucci, S., et al., 2017. Estimating wheat yield in China at the field and district scale from the assimilation of satellite data into the Aquacrop and Simple Algorithm for Yield (SAFY) models. Remote Sensing, 9(6): 509.

Statistics Bureau of Dezhou, Survey Team of Dezhou, 2010, 2014, 2015. Statistics on the production of major agricultural products in each county. Dezhou Statistical Yearbook. (in Chinese)

Statistics Bureau of Liaocheng, 2010, 2014, 2015. Statistics on the production of major agricultural products in each county. Liaocheng Statistical Yearbook. (in Chinese)

Thorp, K.R., Wang, G., West, A.L., Moran, M.S., Bronson, K.F., White, J.W. and Mon, J., 2012. Estimating crop biophysical properties from remote sensing data by inverting linked radiative transfer and ecophysiological models. Remote Sens. Environ. 124, 224–233.

Van Diepen, C.A., Wolf, J., Van Keulen, H., Rappoldt, C., 1989. WOFOST: a simulation model of crop production. Soil Use Manage. 5(1), 16–24.

Verhoef, W. 1984. Light scattering by leaf layers with application to canopy reflectance modeling: the SAIL model. Remote Sens. Environ. 16:125–141.

Verhoef, W. 1985. Earth observation modeling based on layer scattering matrices. Remote Sens. Environ., 17, 165–178.

Verhoef, W. 1998. Theory of radiative transfer models applied in optical remote sensing of vegetation canopies, PhD Thesis, Wageningen Agricultural University, 310 pp.

Wang, D., Wang, J., & Liang, S., 2010. Retrieving crop leaf area index by assimilation of MODIS data into a crop growth model. Science China Earth Sciences, 53(5), 721-730.

Weiss, M., Troufieau, D., Baret, F., Chauki, H., Prevot, L., Olioso, A., Bruguier, N. and Brisson, N., 2001. Coupling canopy functioning and radiative transfer models for remote sensing data assimilation. Agric. For. Meteorol., 108, 113-128.

Welch, G. and Bishop, G. 2006. An Introduction to the Kalman Filter. Department of Computer Science, University of North Carolina, Chapel Hill, Report TR 95-041.

Wu, L., Liu, X.N., Wang, P., Zhou, B.T., Liu, M.L., Li, X.Q., 2013. The assimilation of spectral sensing and the WOFOST model for the dynamic simulation of cadmium accumulation in rice tissues. Internat. J. Appl. Earth Obs. Geoinf. 25, 66–75.

Zhang, L., Guo, C.L., Zhao, L.Y., Zhu, Y., Cao, W.X., Tian, Y.C., Cheng, T., Wang, X., 2016. Estimating wheat yield by integrating the WheatGrow and PROSAIL models. Field Crops Research, 192, 55-66.

Zhou, G., Liu, X., Zhao, S., et al. Estimating fAPAR of rice growth period using radiation transfer model coupled with the WOFOST model for analyzing heavy metal stress. Remote Sensing, 2017, 9(5):424.

Zhu, X., Chen, J., Gao, F., Chen, X., Masek, J. G. 2010. An enhanced spatial and temporal adaptive reflectance fusion model for complex heterogeneous regions. Remote Sens. Environ., 114(11), 2610–2623.

Toshichika I., Masayuki Y., Motoki N. 2009. Parameter estimation and uncertainty analysis of a large-scale crop model for paddy rice: Application of a Bayesian approach[J]. Agricultural & Forest Meteorology,149(2):333-348.

Captions of Figures

Figure 1. Study area. P123R033 and P123R034 represent the two Landsat scenes that covered the study area. These are part of MODIS tiles h26v05 and h27v05.

Figure 2. Daily mean temperature and precipitation of study area in 2009, 2013 and 2014

Figure 3. Profiles of the reflectance values simulated by the coupled WOFOST–PROSAIL model with (a) TSUM1 ranging from 700 to 1300 °C d and (b) the TDWI ranging between 140 and 350 kg·ha-1, (c) SPAN ranging between 23 and 43 days, and (d) LIDF(at vegetation developmental stage 1.3, grain-filling) ranging from –0.95 to 0.85.

Figure 4. Flowchart for the process of assimilating remotely sensed reflectance (ref.) data into the coupled crop growth and radiative transfer model using the 4DVar assimilation algorithm. KF, Kalman filter; SCE–UA, shuffled complex evolution–University of Arizona algorithm. “Clusters” refers to different categories after ISODATA clustering analysis.

Figure 5. Illustration of the grid and cluster strategy for cells in the grid.

Figure 6. Temporal sequences of the spatial variation in the smoothed 500-m MODIS band 2 (NIR, 841–876 nm) surface reflectance and synthetic Kalman filter (KF) Landsat 8 band 5 (NIR, 851-879 nm) surface reflectance from cloud-free images during the winter wheat growing season (using data from 2013 as an example).

Figure 7. The temporal pattern of surface reflectance for a representative pixel based on the synthetic Kalman filter (KF) and the Landsat and MODIS reflectance data, and uncertainty in the Kalman filter value for a given pixel: (a) red: MODIS 500-m band 1 (620–670 nm), synthetic Kalman filter, and Landsat 8 band 4 (636-673 nm); (b) NIR: MODIS 500-m band 2 (841–876 nm), synthetic Kalman filter, and Landsat 8 band 5 (851-879 nm); (c) SWIR: MODIS 500-m band 6 (1628–1652 nm), synthetic Kalman filter, and Landsat 8 band 6 (1566-1651 nm).

Figure 8. Comparison of the reflectance (ref.) simulated by the coupled model and the three kinds of observations. KF, Kalman filter.

Figure 9. Comparisons of the spatial patterns of winter wheat yield simulated by the WOFOST model (a) without data assimilation and (b-d) with assimilation based on three different remotely sensed reflectance datasets. (e) Official statistics for yield in (1) 2009, (2) 2013, and (3) 2014.

Figure 10. Accuracy of the estimated winter wheat yield at a county level in comparison with government statistics. Results are for assimilating the (left) MODIS reflectance, (center) Landsat reflectance, and (right) synthetic Kalman filter reflectance using the 4DVar assimilation strategy for (top) 2009, (center) 2013, and (bottom) 2014.

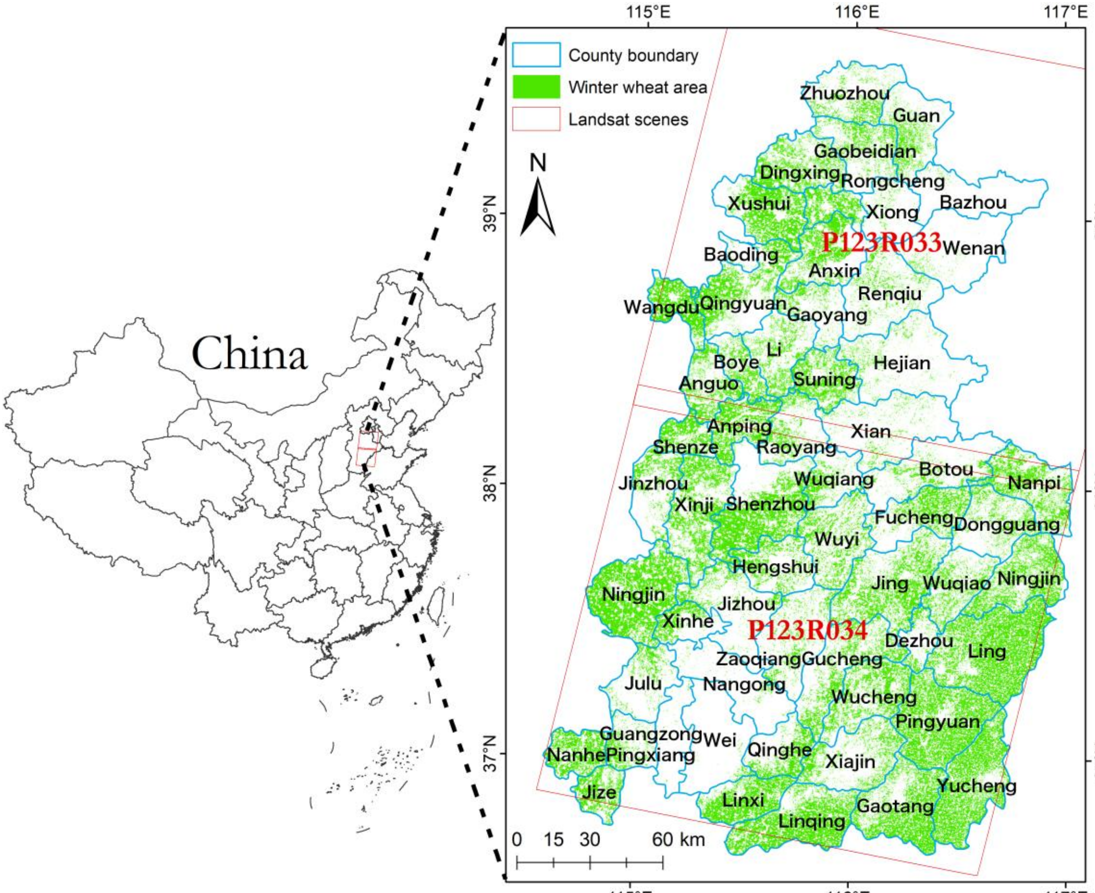

Figure 1. Study area. P123R033 and P123R034 represent the two Landsat scenes that covered the study area. These are part of MODIS tiles h26v05 and h27v05.

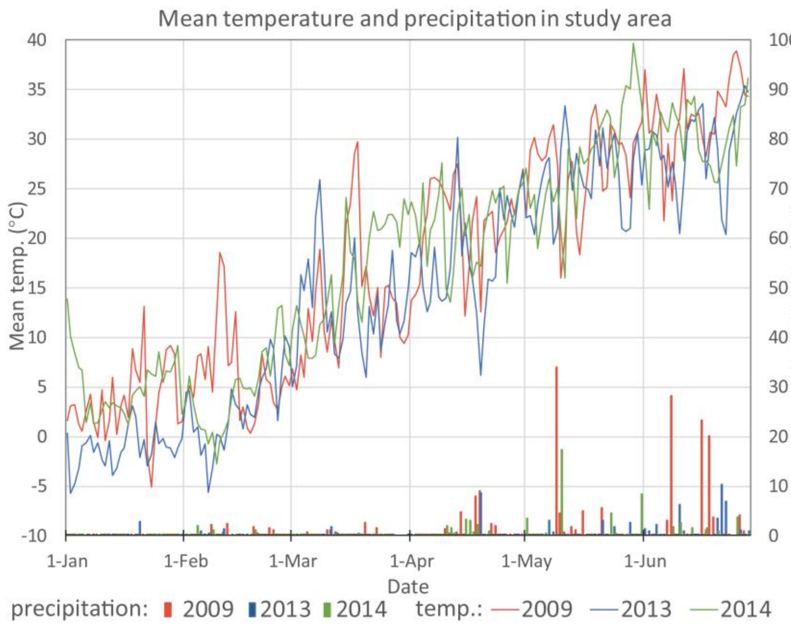

Figure 2. Daily mean temperature and precipitation of study area in 2009, 2013 and 2014

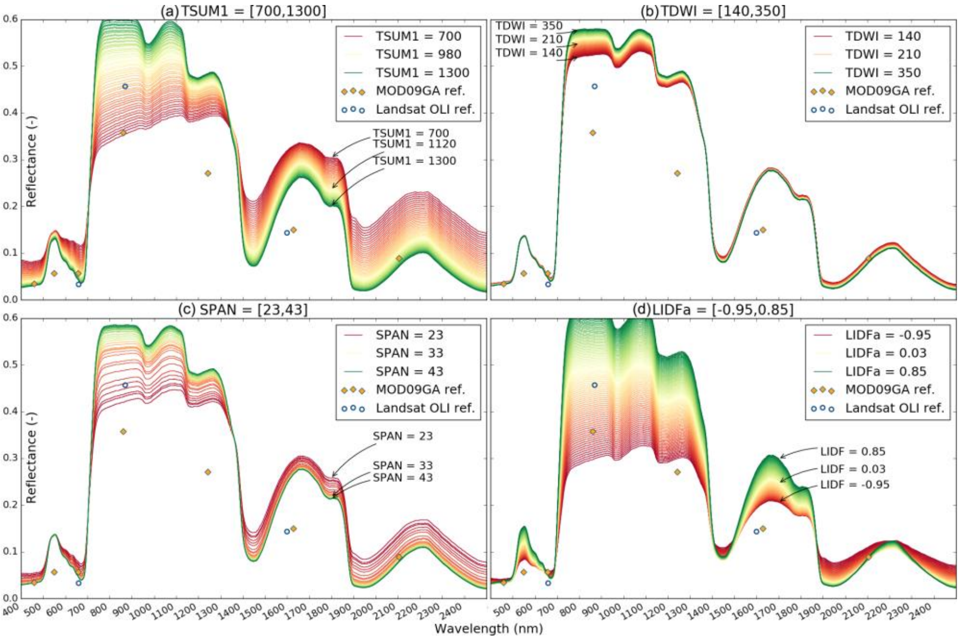

Figure 3. Profiles of the reflectance values simulated by the coupled WOFOST–PROSAIL model with (a) TSUM1 ranging from 700 to 1300 °C d and (b) the TDWI ranging between 140 and 350 kg·ha^{-1}, (c) SPAN ranging between 23 and 43 days, and (d) LIDFa (at vegetation developmental stage 1.3, grain-filling) ranging from –0.95 to 0.85.

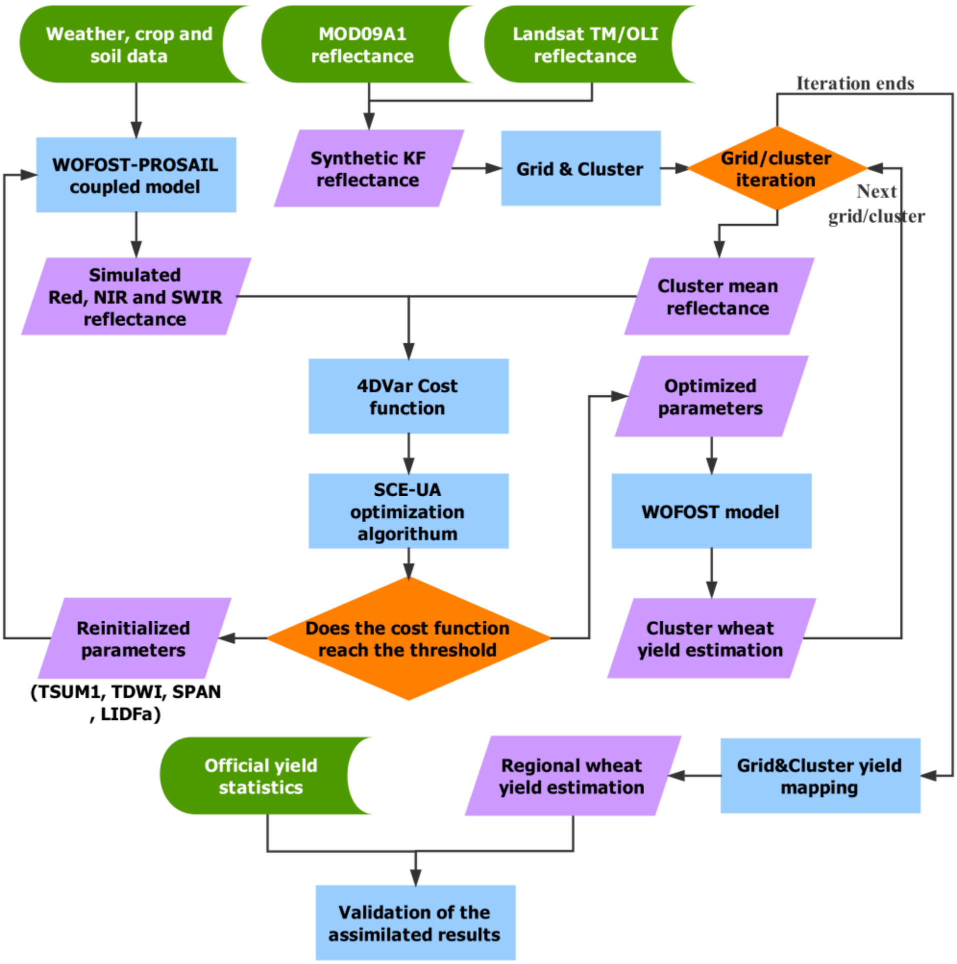

Figure 4. Flowchart for the process of assimilating remotely sensed reflectance (ref.) data into the coupled crop growth and radiative transfer model using the 4DVar assimilation algorithm. KF, Kalman filter; SCE–UA, shuffled complex evolution–University of Arizona algorithm. “Clusters” refers to different categories after ISODATA clustering analysis.

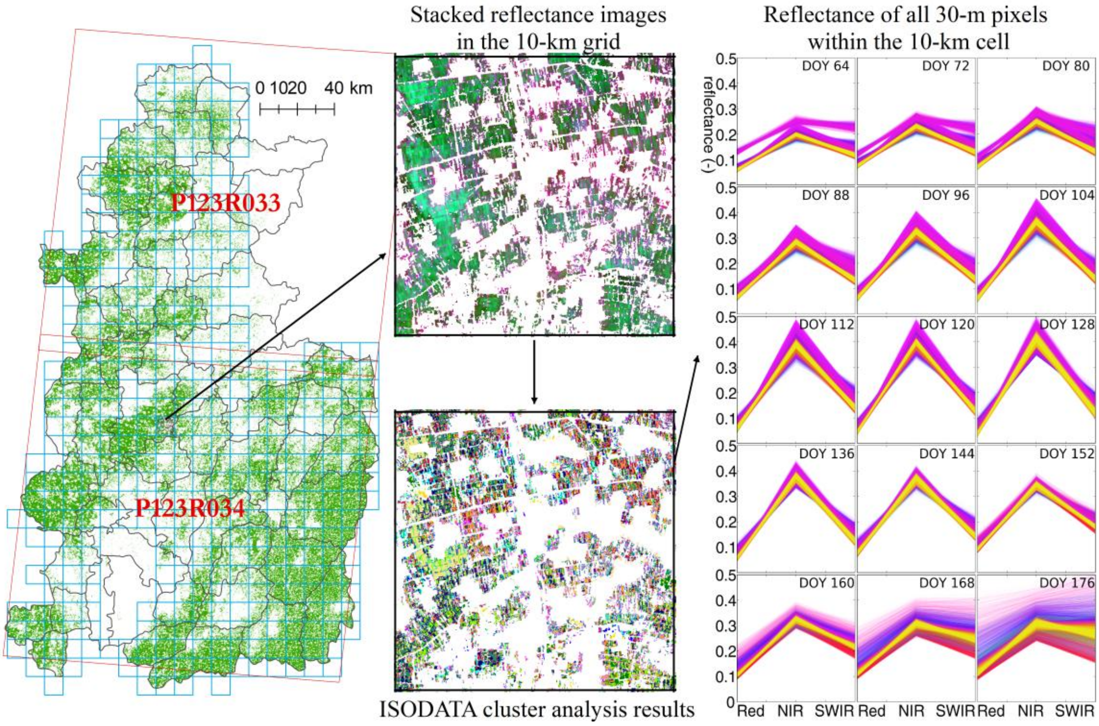

Figure 5. Illustration of the grid and cluster strategy for cells in the grid.

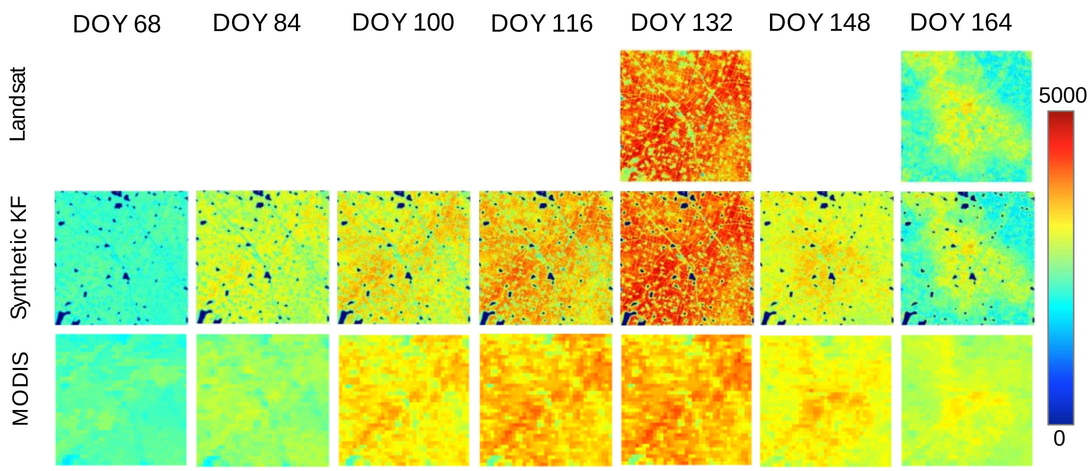

Figure 6. Temporal sequences of the spatial variation in the smoothed 500-m MODIS band 2 (NIR, 841–876 nm) surface reflectance and synthetic Kalman filter (KF) Landsat 8 band 5 (NIR, 851-879 nm) surface reflectance during the winter wheat growing season (using data from 2013 as an example).

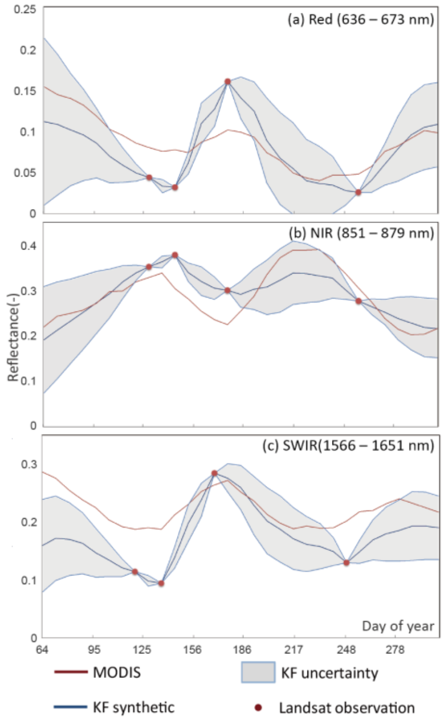

Figure 7. The temporal pattern of surface reflectance for a representative pixel based on the synthetic Kalman filter (KF) and the Landsat and MODIS reflectance data, and uncertainty in the Kalman filter value for a given pixel: (a) red: MODIS 500-m band 1 (620–670 nm), synthetic Kalman filter, and Landsat 8 band 4 (636-673 nm); (b) NIR: MODIS 500-m band 2 (841–876 nm), synthetic Kalman filter, and Landsat 8 band 5 (851-879 nm); (c) SWIR: MODIS 500-m band 6 (1628–1652 nm), synthetic Kalman filter, and Landsat 8 band 6 (1566-1651 nm).

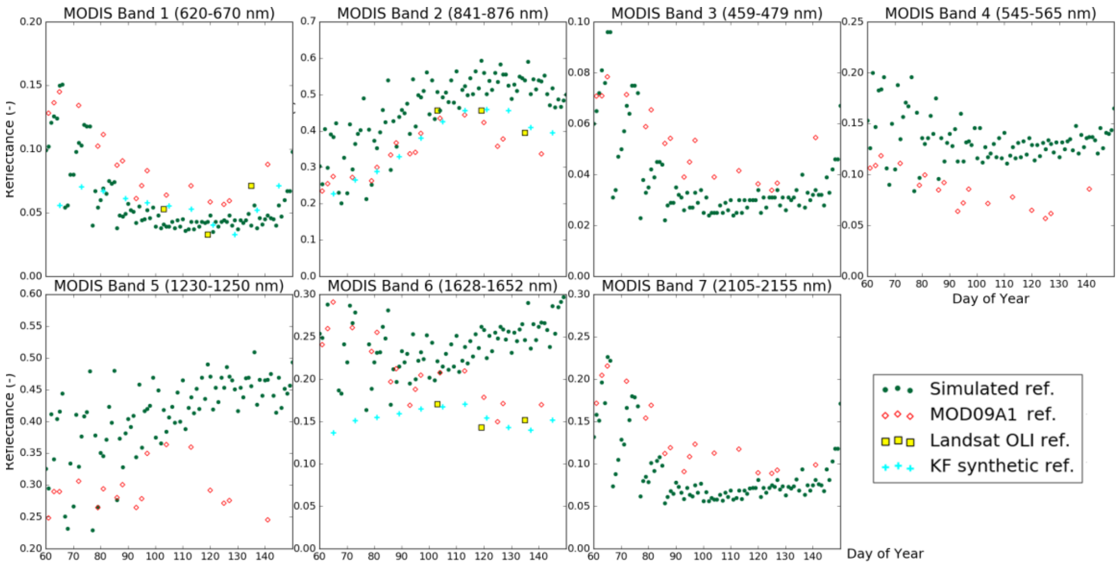

Figure 8. Comparison of the reflectance (ref.) simulated by the coupled model and the three kinds of observations. KF, Kalman filter.

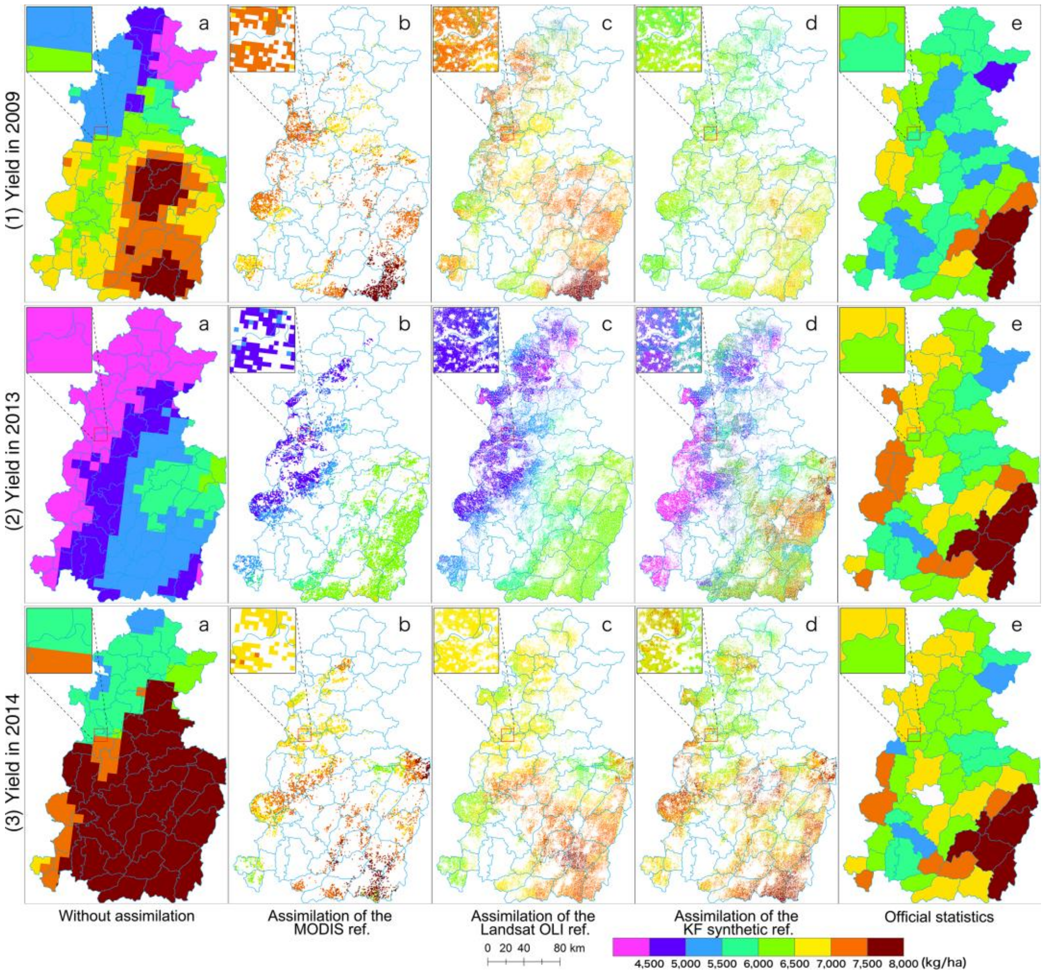

Figure 9. Comparisons of the spatial patterns of winter wheat yield simulated by the WOFOST model (a) without data assimilation and (b-d) with assimilation based on three different remotely sensed reflectance datasets. (e) Official statistics for yield in (1) 2009, (2) 2013, and (3) 2014.

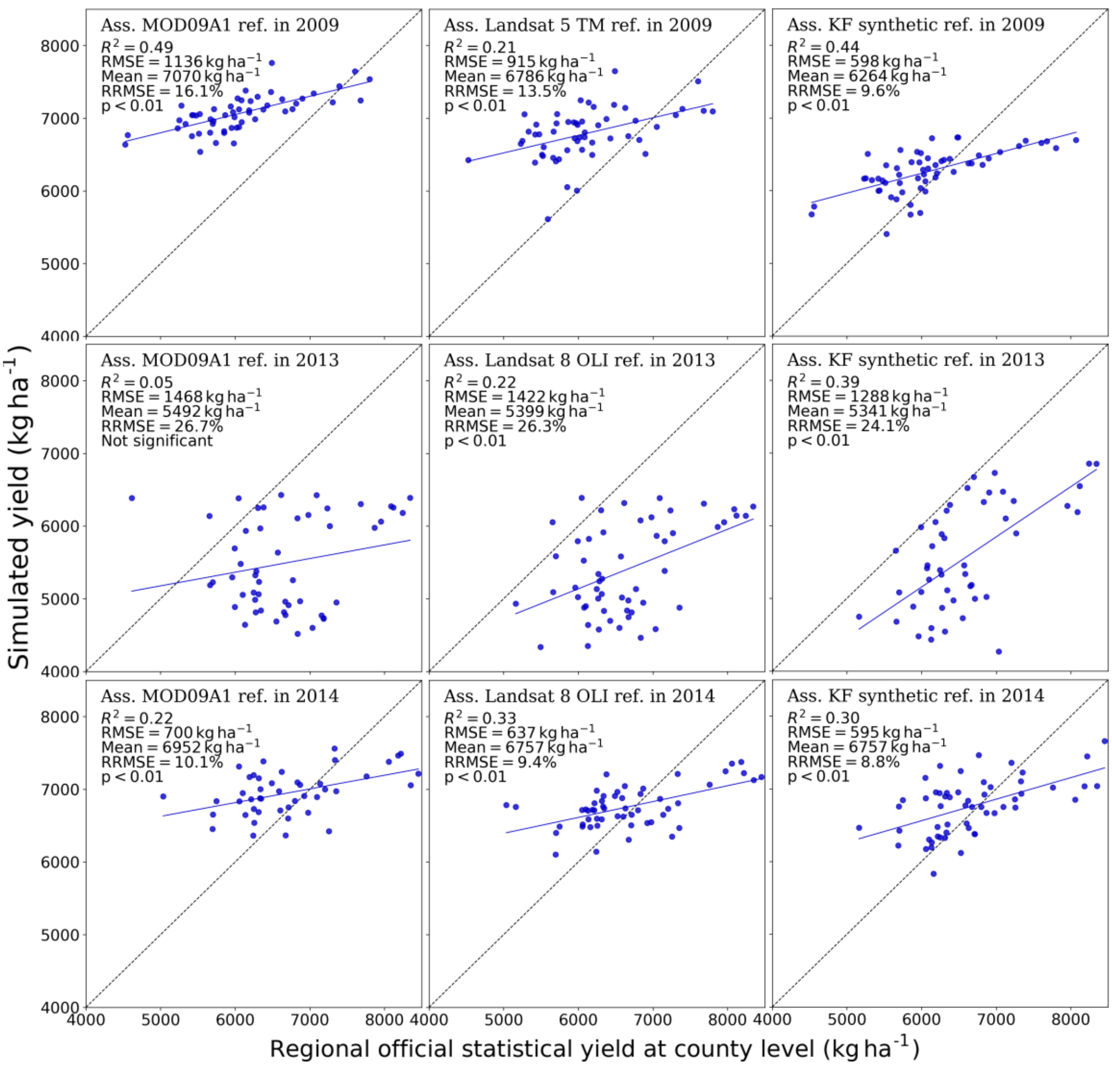

Figure 10. Accuracy of the estimated winter wheat yield at a county level in comparison with government statistics. Results are for assimilating the MODIS reflectance(left column) , Landsat reflectance (center column), and synthetic KF reflectance (right column) using the 4DVar assimilation strategy for the year of 2009 (top row), 2013 (center row), and 2014 (bottom row).

Tables

Table 1 Landsat image acquisition dates during the winter wheat growing season for each path and row.

Landsat scene	2009 Landsat 5 TM	2013 Landsat 8 OLI	2014 Landsat 8 OLI	Total
P123R033	DOY25 winter dormancy	DOY132 anthesis	DOY 103 elongation	9
	DOY41 winter dormancy	DOY164 maturity	DOY 119 booting	
	DOY 73 green-up		DOY135 grain-filling	
	DOY137 grain-filling			
P123R034	DOY25 winter dormancy	DOY116 booting	DOY 103 jointing	10
	DOY41 winter dormancy	DOY132 anthesis	DOY 119 booting	
	DOY 73 green-up	DOY164 maturity	DOY135 grain-filling	
	DOY137 grain-filling			
Total	8	5	6	19

Table 2 Input parameters in the PROSAIL model and data sources.

Parameter	Unit	Range	Data sources
LAI	-	0 to 8	Simulated by WOFOST
C_{ab}	$\mu g \cdot cm^{-2}$	20 to 80	Empirical relationship for the vegetation developmental stage (DVS) in WOFOST
C_m	$\mu g \cdot cm^{-2}$	0.002 to 0.200	Empirical relationship with dry matter of leaf simulated by WOFOST
C_{brown}	$\mu g \cdot cm^{-2}$	0 to 0.2	Linearly associated with C_{ab}
N	-	1.2 to 1.8	Empirical relationship with SLA simulated by WOFOST
LIDFa	-	-1 to 1	Linear interpolation with optimized value through 4DVar assimilation
LIDFb	-	0	Default value
psoil	-	0.5 to 3.5	Empirical relationship with daily precipitation
View zenith	°	0 to 90	from Landsat metadata
Solar zenith	°	0 to 90	from Landsat metadata
Relative azimuth	°	-180 to 180	from Landsat metadata
C_w	cm	0.0185	Empirical value from Zhang et al. (2016)
rsoil	-	1	Default value

Table 3 Comparison of the assimilated wheat yield using the three reflectance datasets with the field-measured yield in 29 sample plots. Significance: ns, not significant; * $p < 0.05$; ** $p < 0.01$

Scheme	Mean (kg/ha)	Max (kg/ha)	Min (kg/ha)	R^2	RMSE (kg/ha)
Field-measured yield at the 29 sample plots	7291	8295	5700	—	—
Simulated yield without data assimilation	7188	8521	6367	0.15 *	808
Simulated yield with assimilation of the MODIS reflectance	7140	7565	6855	0.25 ns	803
Simulated yield with assimilation of the Landsat reflectance from three dates	7009	7255	6761	0.38 **	762
Simulated yield with assimilation of the synthetic Kalman filter reflectance	6579	7250	5760	0.52 **	710